

See discussions, stats, and author profiles for this publication at: <https://www.researchgate.net/publication/265087755>

Surface and Bulk Oxygen Vacancy Defect States near the Fermi Level in 125 nm WO₃Δ/TiO₂ (110) Films: A Resonant Valence Band Photoemission Spectroscopy Study

ARTICLE *in* THE JOURNAL OF PHYSICAL CHEMISTRY C · JULY 2011

Impact Factor: 4.77 · DOI: 10.1021/jp202375h

CITATIONS

3

READS

18

10 AUTHORS, INCLUDING:



[Qianli Chen](#)

Max Planck Institute for Polymer Research

12 PUBLICATIONS 256 CITATIONS

[SEE PROFILE](#)



[Funda Aksoy Akgul](#)

Nigde University

50 PUBLICATIONS 584 CITATIONS

[SEE PROFILE](#)



[Yuan Mao](#)

Zhejiang Normal University

113 PUBLICATIONS 10,422 CITATIONS

[SEE PROFILE](#)



[Thomas Graule](#)

Empa - Swiss Federal Laboratories for Materi...

144 PUBLICATIONS 1,649 CITATIONS

[SEE PROFILE](#)

Surface and Bulk Oxygen Vacancy Defect States near the Fermi Level in 125 nm $\text{WO}_{3-\delta}/\text{TiO}_2$ (110) Films: A Resonant Valence Band Photoemission Spectroscopy Study

Artur Braun,^{*,†,‡} Selma Erat,^{†,§,||} Xiaojun Zhang,^{⊥,♯} Qianli Chen,^{†,∇} Tzu-Wen Huang,[†] Funda Aksoy,^{○,◆} Romy Löhnert,^{†,¶} Zhi Liu,[◆] Samuel S. Mao,^{⊥,♯} and Thomas Graule^{†,⊗}

[†]Laboratory for High Performance Ceramics Empa, Swiss Federal Laboratories for Materials Science and Technology, CH-8600 Dübendorf, Switzerland

[‡]Hawaii Natural Energy Institute, University of Hawaii at Manoa, Honolulu, Hawaii 96822, United States

[§]Department of Materials, ETH Zürich, Swiss Federal Institute of Technology, CH-8093 Zürich, Switzerland

^{||}Advanced Technologies Research & Application Center, Mersin University, TR-33343 Yenisehir, Mersin, Turkey

[⊥]Department of Mechanical Engineering, University of California—Berkeley, Berkeley, California 94720, United States

[#]Environmental Energy Technologies Division, Lawrence Berkeley National Laboratory, Berkeley, California 94720, United States

[∇]Physics Department, ETH Zürich, Swiss Federal Institute of Technology, CH-8093 Zürich, Switzerland

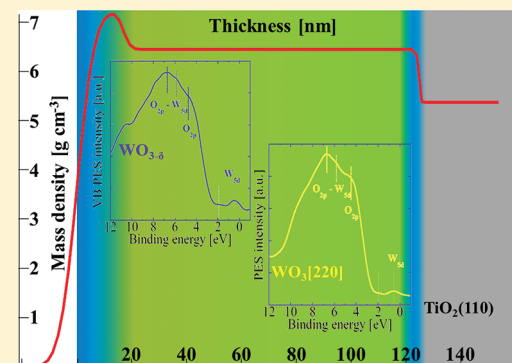
[○]Department of Physics, Cukurova University, TR-01330 Adana, Turkey

[◆]Advanced Light Source, Lawrence Berkeley National Laboratory, Berkeley, California 94720, United States

[¶]Department of SciTec, University of Applied Sciences—Jena, D-07745 Jena, Germany

[⊗]Technische Universität Bergakademie, Freiberg D-09064 Freiberg, Germany

ABSTRACT: An approximately 125 nm thick pulsed laser deposited blue, nonstoichiometric $\text{WO}_{3-\delta}$ film grows on TiO_2 (110) in the [220] direction. Oxidative treatment at 400 °C turns the film color from blue to yellow and improves the film quality considerably, as shown by improvement of the Kiessig oscillations in the X-ray reflectometry curves. Detailed analysis of resonant valence band photoemission spectra of the as-deposited nonstoichiometric blue film and oxidized yellow film suggests that a transition near the Fermi energy originates from the nonstoichiometry, i.e., oxygen deficiency, and insofar poses electronic defect states that partially can be eliminated by heat treatment in oxygen. The defects of the as-deposited blue film seem to be located throughout the film, except for the top surface due to exposure to oxygen in ambient air. Thermal after-treatment under oxygen heals the defects in the bulk, whereas residual defect states appear to remain near the film–substrate interface. Potential strain at the substrate–film interface due to lattice mismatch may be one origin for the remanence of the defect states in the bulk.



INTRODUCTION

The structure and physicochemical properties of tungsten oxide have sparked interest by scientists and engineers for a long time because of its relevance for technological applications as photoelectrochemical cell anodes, gas sensors, and photochromic materials, for example.^{1,2} On the basis of a study of defect-free and altered WO_3 surfaces with photoelectron spectroscopy, it has been speculated that the properties of WO_3 depend critically on the defect states in the bulk and on the surface, rather than on its intrinsic nature.³

An early bulk and surface specific electronic structure study of WO_3 is presented in ref 4, where in particular it was found that the perfect (100) surface has no defect states in the band gap. WO_3 belongs to a class of materials that can tolerate deviations

from stoichiometry by adjustment of oxygen octahedral using shear mechanisms, without formation of oxygen vacancies.³ This was already earlier suggested by Matthias' observation that WO_3 single crystals were remarkably soft.⁵ In the oxygen octahedron, the e_g orbitals ($d_{x^2-y^2}, d_{z^2}$) of W orient directly to the oxygen atoms, whereas the t_{2g} orbitals (d_{xy}, d_{yz}, d_{zx}) point between the coordinating ligands.⁴ The corresponding calculated density of states is illustrated in Figure 3 in ref 4. The defect free (100) surface has a barely noticeable small density of states in the p–d band gap, but surface states can be induced by creating oxygen

Received: March 13, 2011

Revised: June 18, 2011

Published: July 14, 2011

vacancies, i.e., reducing the coordination of W. No surface states should appear within the semiconducting gap of the defect free (001) surface, where W loses no more than one coordinating ligand. Systematic studies showed that Ar^+ bombardment causes an oxygen deficient surface, whereas O^+ bombardment does not.³ It appears that a temperature as high as 400 °C is necessary for reduced WO_3 to incorporate oxygen into the bulk.⁶ An assumption of proportionality between the density of color centers and the density of states contributing to hopping conductivity has been experimentally supported.⁷

Compared with as-deposited WO_3 films, the film postannealed in oxygen shows an improved electric-field-induced resistance switching behavior. On the basis of photoemission data, the resistance switching was attributed to the change in the interfacial barrier potential, due to the electron trapping/detrapping in surface states, and switching improvement was attributed to the decrease in the density of states at surface.⁸

While the energy of bulk WO_3 depends weakly on the distortions and tilting of the WO_6 octahedra, relaxation of the (001) surface results in a significant decrease of surface energy, accompanied by a dramatic redistribution of the density of states near the Fermi level. This redistribution is responsible for the decrease of electronic energy.⁹

Composites of WO_3 and TiO_2 have been of interest for example in photocatalysis. Improved photocatalytic activity of WO_3/TiO_2 composite nanoparticles has been attributed to the increased surface acidity and better charge separation due to the coupling of WO_x species and TiO_2 .¹⁰ Thin TiO_2/WO_3 multi-layers made with pulsed laser deposition (PLD) on silicon and quartz substrates have higher photocatalytic activity in visible light than TiO_2 alone, with 5% WO_3 having the maximum activity.¹¹ Epitaxial WO_3 films appear to have a better conductivity and H_2S gas sensing response than polycrystalline films¹² and can be synthesized for thicknesses up to 700 nm on SrTiO_3 (001).¹³

On the initial stage of reduction of hexagonal tungsten trioxide, h- WO_3 , the nonstoichiometric h- $\text{WO}_{2.8}$ phase was synthesized. The formation of an additional near-Fermi subband, absent in the XPS VB spectrum of h- WO_3 , was observed on the nonstoichiometric h- $\text{WO}_{2.8}$. Half-widths of the structures in XPS VB and W 4f and O 1s core-level spectra increase somewhat when going from h- WO_3 to h- $\text{WO}_{2.8}$.¹⁴

The present study deals with the location of oxygen defects and their corresponding defect states in an approximately 125 nm thin $\text{WO}_{3-\delta}$ film deposited on single crystal TiO_2 and a thermal oxidative after-treatment, and its spectroscopic assessment with valence band photoemission spectroscopy.

■ EXPERIMENTAL SECTION

Compact films of approximately 125 nm thickness were deposited on single crystal TiO_2 substrates with (110) orientation (CRYSTEC, Berlin) by pulsed laser ablation from a WO_3 target (99.9% purity, American Elements) with 580 °C substrate temperature and 10 mTorr oxygen partial pressure. The excimer laser (Lambda Physik LPX 210i, 248 nm wavelength) was run at a pulse energy of 160 mJ and a repetition rate of 10 Hz. The deposition time was 15 min. The films had a bluish color after deposition (as deposited). For comparison, the films deposited at 100 mTorr oxygen partial pressure at 300 °C on glass substrates were found to be near-stoichiometric monoclinic WO_3 .¹⁵ An aliquot of the film was heated in a tube furnace for 48 h at 400 °C

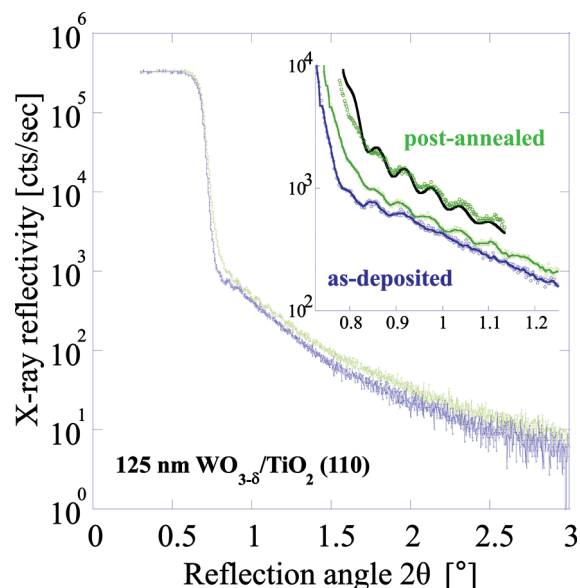


Figure 1. X-ray reflectograms for the as-deposited (blue, lower) and postannealed (yellow, top) film on TiO_2 (110). The inset shows a magnification of the range with oscillations and a simulated reflectogram for the postannealed film (solid line).

in 100 mL/min oxygen flow, after which the color of the film had turned to a light yellow (postannealed). The films were subject to X-ray diffraction and X-ray reflectometry (Philips X'pert, Cu K α). Photoemission spectra were recorded at end station¹⁶ at beamline 9.3.2 of the Advanced Light Source, Lawrence Berkeley National Laboratory. The energy resolution of the beamline is $E/\Delta E = 3000$.¹⁷ The XPS survey scans (not shown here), show the presence of carbon (C1s) on both films, more so for the as-deposited film than for the postannealed film. Surface treatment was not undertaken so as to preserve the surface structure for this study.

■ RESULTS AND DISCUSSION

Reflectometry. The X-ray reflectometry curves in Figure 1 show intensity oscillations in the range $0.79^\circ < 2\theta < 1.2^\circ$ for the as-deposited (lower curve, blue) and for the postannealed, oxidized film (upper curve, yellow). The as-deposited film shows four intensity maxima in the range 0.8° to 1.0° . The postannealed film has more pronounced oscillations with maxima ranging from 0.8° to 1.2° , indicating that the film surface roughness and interface roughness decrease upon thermal oxidative after-treatment, leading to an overall improvement of the film quality. In contrast, thermal oxidative treatment of 50 nm thin lithiated WO_3 up to 350 °C led to rougher surfaces.¹⁸ The oscillations of the oxidized film move to slightly larger angles, suggesting a slight overall increase of film thickness upon oxidation. It was not possible to completely model the reflectivity curves, suggesting that simple bilayers or diffuse layers were not representative of our films. The inset in Figure 1 shows part of the reflectogram of the postannealed film and the simulated reflectogram, in addition to the magnification of the reflectograms of as-deposited and postannealed film. Best fit results were obtained with a film thickness of 121 nm for the as-deposited film with a surface roughness of 8.3 nm, and 125 nm for the postannealed film with a surface roughness of 5 ± 0.5 nm. From the simulation of the

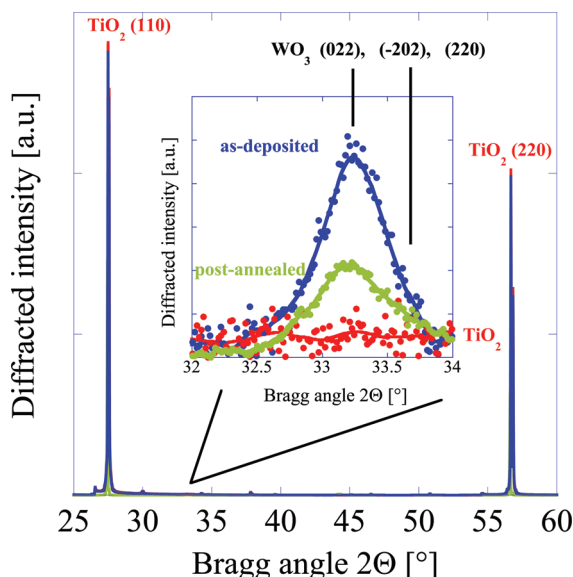


Figure 2. X-ray diffractograms for the TiO_2 (110) substrate (red thin line) and the 125 nm as-deposited (blue thick line) and postannealed (yellow thick line) $\text{WO}_{3-\delta}$ film.

reflectograms we estimated that the surface of the postannealed film had 15 nm thick a top layer of substoichiometric $\text{WO}_{3-\delta}$ and a 110 nm bulk layer of virtually stoichiometric WO_3 . The interface between top layer and bulk has an approximate roughness of 2 ± 0.5 nm. The interface between bulk WO_3 and TiO_2 substrate is approximately 0.2 ± 0.02 nm.

X-ray Diffraction. Figure 2 shows the X-ray diffractogram of the as-deposited film on the TiO_2 (110) substrate. The strong lines at around 28° and 57° are the (110) and (220) Bragg reflections of the substrate (JCPDS 08-0739), respectively. The small, broad peak at about 33.3° , magnified in the inset, is commensurate with the WO_3 (022) Bragg reflection (JCPDS 08-0745), suggesting that the WO_3 film grows with (022) orientation on the substrate and maintains this orientation also after postannealing (JCPDS 24-0747). The film has monoclinic symmetry and lattice parameters $a = 0.7595$ nm, $b = 0.7638$ nm, and $c = 0.3995$ nm. The conjugated (044), (404), and (440) reflections, not shown here, were also identified. No other Bragg reflections indicative to WO_3 could be made out. The 200–500 nm films grown by Ramana et al.¹⁵ showed over a dozen different reflections, which suggested there was no strong preferential orientation. In contrast, reactive sputtering of W in 1.5 mTorr O_2 pressure onto LaAlO_3 (100) at 873 K produced approximately 125 nm films with [100] direction.¹⁹

X-ray Spectroscopy. The X-ray photoelectron spectra (XPS) of the as-deposited film in Figure 3 show the valence band (VB) region near the Fermi energy (E_F) for excitation energies from 270 to 700 eV. The high intensity of the spectrum at +12.3 eV recorded at $E_{\text{kin}} = 270$ eV is potentially due to resonance enhancement of a O 2p–W 6s derived feature. The flat, featureless intensity plateau region between +10 eV and +5 eV is known for $\text{WO}_{3-\delta}$.

Upon increasing E_{kin} to 400 eV, additional features become apparent in the VB region. Five features remain noticeable up to $E_{\text{kin}} = 700$ eV. The small, low intensity yet noticeable peak right at $\text{VBM} = 0$, as will be shown later, originates from defect states related to oxygen deficiency.^{3,4} At +5 eV, already at the onset of

significant density of states (DOS), a shoulder or kink is indicative of a transition and can be assigned to W^{5+} in oxygen deficient, blue $\text{WO}_{3-\delta}$. We will see later that the more stoichiometric WO_3 with yellow color has a similar shoulder for W^{6+} at +4 eV, corroborating the previously observed shift of VB spectra upon reduction or oxidation. The O 2p bonding peak presents the virtually absolute intensity maximum in the VB DOS at around +6 to +7 eV. A very pronounced peak at +10 to +12 eV is known for many metal oxides as indicative of a ligand-to-metal charge transfer satellite (LMCT) or an O 2p–W 6s transition. In the latter case, e_g orbitals ($d_{x^2-y^2}$ and d_{z^2}) of W point directly to the surrounding oxygen atoms, whereas the t_{2g} orbitals (d_{xy} , d_{yz} , d_{zx}) point between the coordinating ligands.⁴ This peak intensity is decreasing with increasing E_{kin} . Increasing E_{kin} causes an increase of the photoelectron mean free path and thus the probing depth. Therefore, the resonant peak at +12.3 eV binding energy obtained with $E_{\text{kin}} = 270$ eV has probably the same electronic origin as the peak that is shifting to around +10.5 eV when E_{kin} increases. Comparing the absolute spectral intensities, we note resonance enhancement not only at $E_{\text{kin}} = 270$ eV (maybe from a W 4d derived resonant LMCT) but also at $E_{\text{kin}} = 525$ eV, which is an O 1s resonant enhancement for the $\text{VBM} = 0$ eV peak and thus likely originates from an oxygen vacancy defect state transition. The reason for the resonance enhancement at $E_{\text{kin}} = 700$ eV is possibly related to an oxygen KVV Auger transition (electron transition from valence band to core hole, K level). Note that the defect peak at $\text{VBM} = 0$ eV is entirely absent for $E_{\text{kin}} = 270$ eV, suggesting that at the film surface region we have no or less such oxygen vacancies, likely because of saturation with oxygen from air at the WO_3 surface. This is why particularly quantitative surface studies on tungsten oxide must be carried out with utmost care to prevent aging or radiation damage.²⁰

Overall it appears that the peak at +12.3 eV shifts with increasing E_{kin} toward smaller binding energies. Because the small extra peak near $\text{VBM} = 0$ is absent at 270 eV, but increasing in intensity with increasing kinetic energy E_{kin} , i.e., having depth sensitivity, it seems that the defect state originates not from the film surface or near-surface region, but from the structure in the bulk of the film or from the film–substrate interface region. Oxidation or reduction of tungsten oxide films not only changes their conductivity, which is related to the film color through the W^{5+} concentration, but also changes the surface structure in a dramatic way.¹⁹ For example, reduction of the $p(2 \times 2)$ surface causes W^{5+} migration into the bulk, leaving vacancies on the surface that organize into ordered troughs to form the $p(4 \times 2)$ strand-terminated surface.¹⁹

The right panel in Figure 3 shows the PES region of the as-deposited films magnified around the VBM. The calculated DOS in ref 4 suggests a broad set of e_g orbital symmetry transitions near E_F , covering a spectral range of around 3–4 eV. Experimental spectra (Figures 4 in refs 3, 21, and 22 and Figure 5 in ref 4) show that the region between the t_{2g} peak and E_F has probably up to four transitions, i.e., two doublets particularly discernible for 600 eV, which we have taken into account for spectral deconvolution. Bringans et al.³ interpret a similar structure at around 2 eV above the Fermi energy as a satellite from He II excitation. We used Voigt functions with 70% Gaussian with a width of 0.4 eV for the two transitions next to E_F , and 0.65 eV for the two subsequent transitions. The relative height (H), energy position (E), and width (σ) of each peak are summarized for the excitation energies in Table 1. A general observation is that the four transitions at

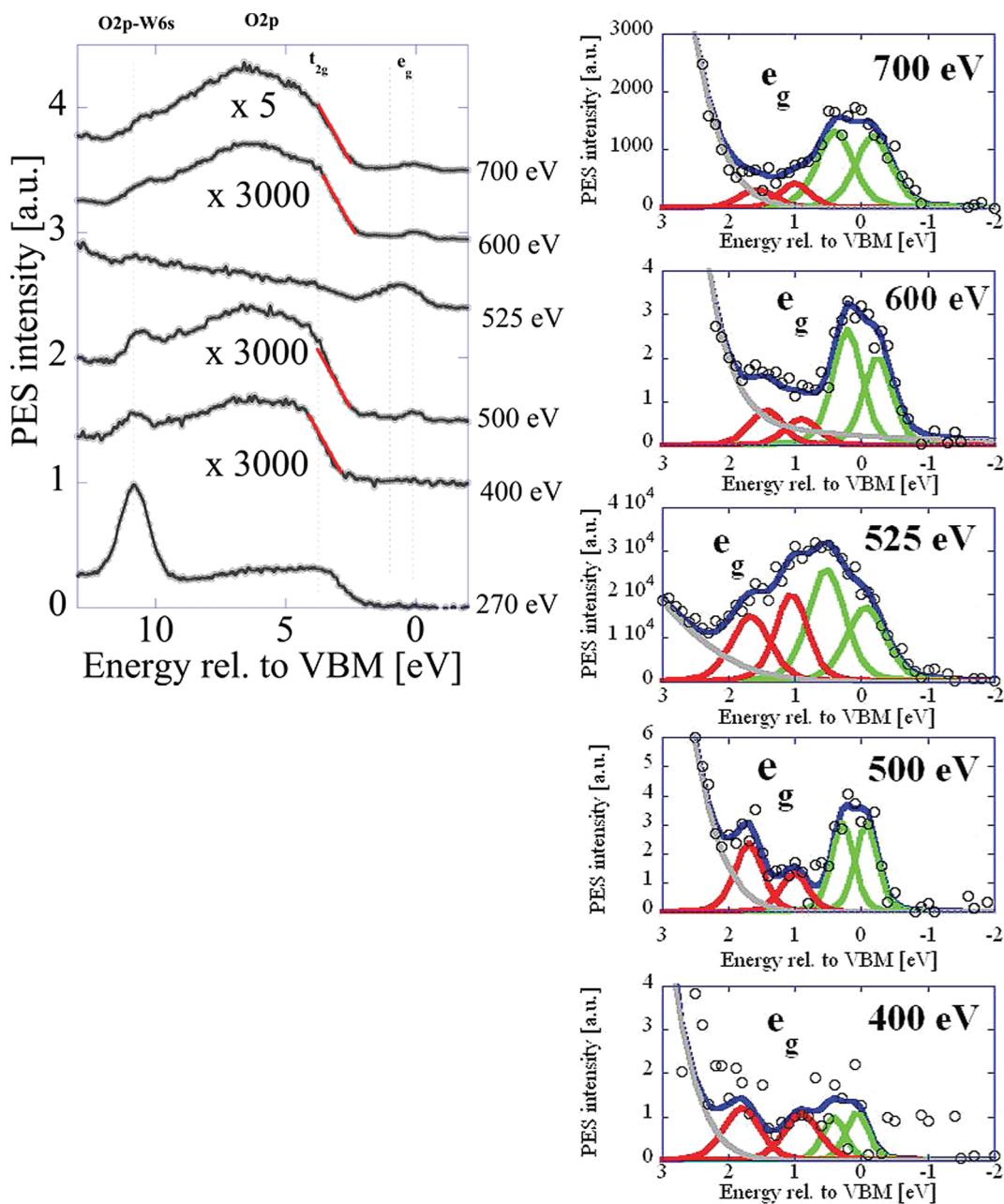


Figure 3. Left: VB PES spectra of the as-deposited film for excitation energies from 270 to 700 eV. Right: Magnification of the spectral range near the Fermi energy with deconvolution of the defect states.

Table 1. Fit Parameters for Deconvolution of e_g Orbital Symmetry Peaks near E_F

E_0	H_1	E_1	σ_1	H_2	E_2	σ_2	H_3	E_3	σ_3	H_4	E_4	σ_4
400	1.1	-0.06	0.4	1.0	0.41	0.4	1.1	0.9	0.65	1.2	1.8	0.65
500	2.8	-0.08	0.5	2.6	0.3	0.5	1	1.1	0.6	2.5	1.76	0.6
525	17000	-0.07	0.7	26000	0.52	0.66	20000	1.05	0.58	15000	1.67	0.7
600	2.02	-0.25	0.51	2.64	0.21	0.53	0.6	0.90	0.6	0.8	1.43	0.6
700	1200	-0.18	0.65	1300	0.39	0.65	424	1	0.55	315	1.57	0.65

525 eV have a very high intensity; i.e., they are affected to the same extent from the resonance enhancement. For the spectra recorded at this X-ray energy, it was necessary for a good fit to employ a larger width in the deconvolution than in the other spectra.

Deconvolution had been made in Figure 12 of ref 22 for the structure between -1.0 eV and E_F in $\text{Na}_{0.5}\text{WO}_3$, the width of which was found to be around 0.85–1.00 eV, depending on whether instrument resolution was taken into account. Our two

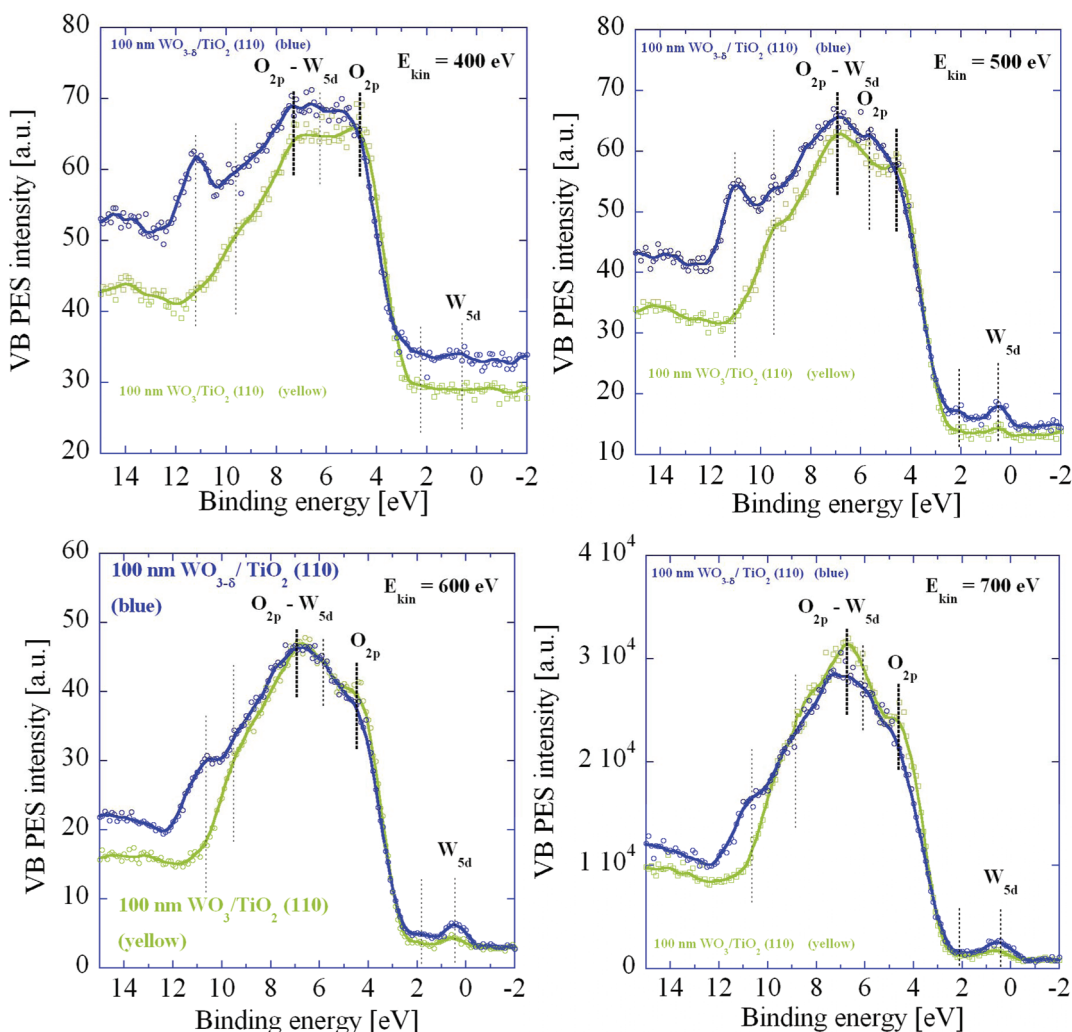


Figure 4. Comparison of VB PES spectra of as-deposited (blue) and postannealed (yellow) films for excitation energies 400–700 eV.

sets of transitions add up each to around 1 for the width, except for the strong resonant signals at 525 and 700 eV excitation energy. Another observation is that the two transitions next to the E_F are larger than the two others particularly for the higher excitation energies. Their relative intensity is increasing with increasing excitation energy, supporting the previous suggestion that in deeper regions of the as-deposited tungsten oxide film we have a higher oxygen vacancy concentration than at the surface region. These deeper regions include the bulk and likely also the substrate–film interface region.

An interpretation of the results is thus that the as-deposited PLD film does not correspond to its blue color and that the surface of the film due to exposure to ambient air may have picked up oxygen and reacted toward somewhat more stoichiometric tungsten oxide.

We now turn to the spectra of the postannealed film, which are compared with the spectra of the as-deposited film in Figure 4. The spectra of the as-deposited and postannealed films generally overlap and show the same global variation of intensity across resonance thresholds. But we notice peculiar differences. The resonance at +10.5 eV is in the as-deposited films more developed than in the postannealed films, particularly for excitation energies of 400 and 500 eV. The postannealed films have no

distinct peak at this energy, but just a shoulder. Such a shoulder is clearly visible in the VB-PES spectrum of an in vacuo fractured WO_3 single crystal (spectrum L in Figure 4 of ref 23). This transition belongs to the p-like valence band.⁴ The defect states near the Fermi energy in the range up to +2 eV in the postannealed films have less spectral weight than those in the as-deposited film, supporting the suggestion that the oxidation during postannealing has filled oxygen vacancies, and thus consequently removed the defect states associated with oxygen vacancies to a considerable extent. It was therefore not possible to carry out a meaningful deconvolution of the spectra of the postannealed film near the Fermi energy.

This process goes along with partial reoxidation of the tungsten ions, as evidenced by the $\text{W} 4f$ core level XPS spectra in Figure 5. The spectrum of the postannealed film has been deconvoluted and labeled the same way as in Figure 4 of ref 24. The doublet 2, 2* is indicative of W^{6+} , and the doublet 1, 1* is indicative of W^{5+} . Components 3, 3* are supposed to arise from surface defects.⁴ The finite spectral weight of 1, 1* and 3, 3* shows that the postannealed film contains a noticeable portion of tungsten in the W^{5+} oxidation state plus surface defects, notwithstanding that W^{6+} is the major species. The core level spectrum of the as-deposited film has more spectral weight at

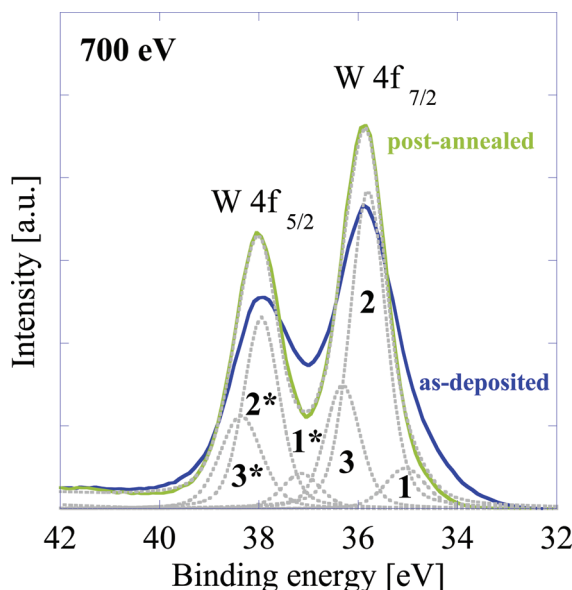


Figure 5. W 4f core level spectra of as-deposited (blue) and post-annealed (yellow) films. Peaks labeled 1, 1* signify W^{5+} , and 2, 2* signify W^{6+} . Peaks 3, 3* arise from surface defects.⁴ Peak assignment according to ref 24.

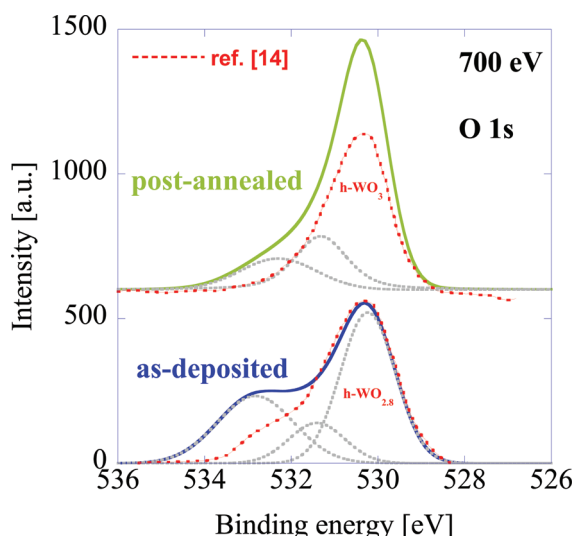


Figure 6. Oxygen 1s core level spectra of the as-deposited and post-annealed films (thick solid lines bottom and top), their convoluted Gaussians (gray dotted lines), and the traced spectra of (red dashed lines). h-WO_{2.8} and h-WO₃ from Figure 7 in ref 14.

the lower energy flanks of the W 4f doublet, revealing a relatively larger portion of W^{5+} in the film. In addition, we see a slight broadening of the spectrum toward the higher energy flanks, suggesting that the relative portion of surface defects in the as-deposited film is larger than in the post-annealed film. This suggestion is supported by the X-ray reflectometry data in Figure 1, where the surface roughness of the postannealed film is lower than in the as-deposited film. Such surface roughness is a manifestation of disorder, and disorder in substoichiometric tungsten oxide films has been observed and assigned to reduced photocurrents.²⁵

The corresponding oxygen 1s core level spectra in Figure 6 are virtually reminiscent of h-WO₃ and h-WO_{2.8} in Figure 7 of ref 14. For the as-deposited film we see identify two clear structures at around 533 and 530.5 eV, the latter one being dominant. The postannealed spectrum shows predominantly only the feature at 530.5 eV, and a yet visible shoulder at 533 eV. While the two structures are clear to make out, deconvolution required actually a third structure at around 531.5 eV.

Such deconvolution with three components has been made for the O 1s spectrum of a 200 nm thin WO₃ film obtained by electron beam evaporation.²⁶ In that study it was found that W exists as 4d on the surface, but at a depth of 10 nm, 4d and also 4f states were observed.

CONCLUSION

Tungsten oxide deposited to approximately 125 nm by laser ablation from a ceramic WO₃ target on TiO₂ (110) grows in [220] crystallographic orientation, as evidenced by X-ray diffraction. Upon thermal oxidative after-treatment, the film surface roughness decreases and the film quality apparently improves, as shown by X-ray reflectivity. The photoemission spectra reveal that the defect states known from oxygen nonstoichiometry in tungsten oxide are located preferentially in the bulk and possibly also in the film–substrate interface region. Exposure to ambient air possibly fills part of the oxygen vacancies at the film surface, and thermal oxidative after-treatment extends the region of filled oxygen vacancies toward the film interior, whereas even extensive oxidation for 48 h under thermal activation at 400 °C is apparently not sufficient to completely fill the oxygen vacancies and remove the prominent defect states near the Fermi energy in the film interior, as evidenced by detailed analysis of the VB PES and core level spectra. A potential structural origin of this behavior is that the lattices of film and substrate are mismatched, and that the substrate imposes a structure on the film at the interface, which favors oxygen deficiency in the interface region of the film to an extent that even excess oxygen at the film surface at elevated temperatures does not fill these vacancies. Possibly this could be a method to design interfaces with an oxygen vacancy concentration robust toward thermal excitation and oxygen gradients.

AUTHOR INFORMATION

Corresponding Author

*E-mail: artur.braun@alumni.ethz.ch. Phone +41 58 765 4850. Fax +41 58 765 4150.

ACKNOWLEDGMENT

The research leading to these results received funding from the European Community's Sixth Framework Marie Curie International Reintegration Program grant no. 042095 (HiTempEchem - X-ray and Electrochemical Studies on Solid Oxide Fuel Cells and Related Materials), Seventh Framework Program Novel Materials for Energy Applications grant no. 227179 (NanoPEC - Nanostructured Photoelectrodes for Energy Conversion), Swiss National Science Foundation grants 200021-116688, 200021-132126, 206021-121306, and IZK0Z2-133944, Swiss Federal Office of Energy contracts 152316-101883, 153613-102809, and 153476-102691, and Empa Board of Directors 7th

R&D Grant. The ALS is supported by the Director, Office of Science/BES, of the U.S. DoE, No. DE-AC02-05CH11231.

■ REFERENCES

- (1) Granqvist, C. G. *Sol. Energy Mater. Sol. Cells* **2000**, *60*, 201–262.
- (2) Deb, S. K. *Sol. Energy Mater. Sol. Cells* **2008**, *92*, 245–258.
- (3) Bringans, R. D.; Höchst, H.; Shanks, H. R. *Phys. Rev. B* **1981**, *24*, 3481–3489.
- (4) Bullett, D.W. J.; Phys., C *Solid State Phys.* **1983**, *16*, 2197–2207.
- (5) Matthias, B. T. *Phys. Rev.* **1949**, *76*, 430–431.
- (6) Schiavello, M.; Pepe, F.; Cannizzaro, M.; de Rossi, S.; Tilley, R. J. D. *Z. Phys. Chem.* **1977**, *106*, 45–51.
- (7) Heinz, B.; Mørz, M.; Widmayer, P.; Ziemann, P. *J. Appl. Phys.* **2001**, *90*, 4007–4018.
- (8) Shang, D. S.; Shi, L.; Sun, J. R.; Shen, B. G.; Zhuge, F.; Li, R. W.; Zhao, Y. G. *Appl. Phys. Lett.* **2010**, *96*, 072103.
- (9) Yakovkin, I. N.; Gutowski, M. *Surf. Sci.* **2007**, *601*, 1481–1488.
- (10) Akurati, K. K.; Vital, A.; Dellemann, J.-P.; Michalow, K.; Graule, T.; Ferri, D.; Baiker, A. *Appl. Catal. B: Environ.* **2008**, *79*, 53–62.
- (11) Shinguu, H.; Bhuiyan, M. M. H.; Ikegami, T.; Ebihara, K. *Thin Solid Films* **2006**, *506–507*, 111–114.
- (12) LeGore, L. J.; Greenwood, O. D.; Pauls, J. W.; Frankel, D. J.; Lad, R. J. *J. Vac. Sci. Technol.* **1997**, *A 15*, 1223–1227.
- (13) Garg, A.; Leake, J. A.; Barber, Z. H. *Phys. D: Appl. Phys.* **2000**, *33*, 1048–1053.
- (14) Solonin, Y. M.; Khyzhun, O. Y.; Graivoronskaya, E. A. *Growth Design* **2001**, *1* (6), 473–477.
- (15) Ramana, C. V.; Utsunomiya, S.; Ewing, R. C.; Julien, C. M.; Becker, U. *J. Phys. Chem. B* **2006**, *110*, 10430–10435.
- (16) Grass, M. E.; Karlsson, P. G.; Aksoy, F.; Lundqvist, M.; Wannberg; Mun, B. S.; Hussain, Z.; Liu, Z. *Rev. Sci. Instrum.* **2010**, *81*, 053106.
- (17) Hussain, Z.; Huff, W. R. A.; Kellar, S. A.; Moler, E. J.; Heimann, P. A.; McKinney, W.; Padmore, H. A.; Fadley, C. S.; Shirley, D. A. *J. Electron Spectrosc. Relat. Phenom.* **1996**, *80*, 401–404.
- (18) Maaza, M.; Gorenstein, A.; Sella, C.; Bridou, F.; Pardo, B.; Corno, J.; Roger, G.; Bohnke, O.; Julián, C. *MRS Proceedings* **1994**, *369*, 125. MRS Fall Meeting Symposium U, Solid State Ionics IV, Editors: Gholam-Abbas Nazri, Jean-Marie Tarascon, Martha Schreiber.
- (19) Li, M.; Altman, E. I.; Posadas, A.; Ahn, C. H. *Thin Solid Films* **2004**, *446*, 238–247.
- (20) Weinhardt, L.; Blum, M.; Baer, M.; Heske, C.; Cole, B.; Marsen, B.; Miller, E. L. *J. Phys. Chem. C* **2008**, *112*, 3078–3082.
- (21) Masek, K.; Nemsak, S.; Mravcakova, M.; Skala, T.; Skoda, M.; Matolin, V. *J. Phys. C: Conf. Ser.* **2008**, *100*, 012008.
- (22) Benbow, R. L.; Hurých, Z. *Phys. Rev. B* **1978**, *17* (12), 4527–4536.
- (23) Himpel, F. J.; Morar, J. F.; McFeely, F. R.; Pollak, R. A. *Phys. Rev. B* **1984**, *30* (12), 7236–7241.
- (24) Bittencourt, C.; Felten, A.; Mirabella, F.; Ivanov, P.; Llobet, E.; Silva, M. A. P.; Nunes, L. A. O.; Pireaux, J. J. *J. Phys.: Condens. Matter* **2005**, *17*, 6813–6822.
- (25) Marsen, B.; Cole, B.; Miller, E. L. *Sol. Energy Mater. Sol. Cells* **2007**, *91*, 1954–1958.
- (26) Ahsan, M.; Tesfamichael, T.; Bell, J.; Blackford, M. G. Microstructural characterization of electron beam evaporated tungsten oxide films for gas sensing applications. In *Proceedings of the 16th AINSE Conference on Nuclear and Complementary Techniques of Analysis*, 25–27 November 2009, Sydney, Australia.